2022 IEEE 5th International Conference on Soft Robotics (RoboSoft)
April 4-8, 2022, Edinburgh, UK

A Simulation-Based Toolbox to Expedite the Digital Design of Bellow Soft Pneumatic Actuators

Yao Yao[1], Liang He[1*] and Perla Maiolino[1]

***Abstract*— Task-oriented applications of soft pneumatic actuators (SPAs) are growing, as digital design and rapid prototyping allow the actuator to be customised. The bellow SPA is promising for current soft material 3D printing due to small material stretch during actuation, yet the complex geometry causes challenges in physical modelling and design. This article provides the users with an open-source toolbox of simulation for a standardised bellow soft pneumatic actuator that can be 3D printed to expedite the design process. Based on MATLAB and COMSOL Multiphysics, the toolbox allows users to customise design features, automatically generate the CAD and then simulate the actuators' performance. It provides two methods to analyse the design: 1) a theoretical modelling method to quickly generate the actuator's workspace with interactive results, 2) a finite element method to evaluate in detail the actuator's deformation and force performance as well as the mechanical properties. The modelling is introduced and validated by comparing the experimental results of 3D printed bellow actuator prototypes with simulation results for angular deflection and blocked force. The maximum root-mean-square error for the theoretical modelling of deformation, finite element method of deformation and force are 9.00°, 7.40° and 1.66 g, respectively.**

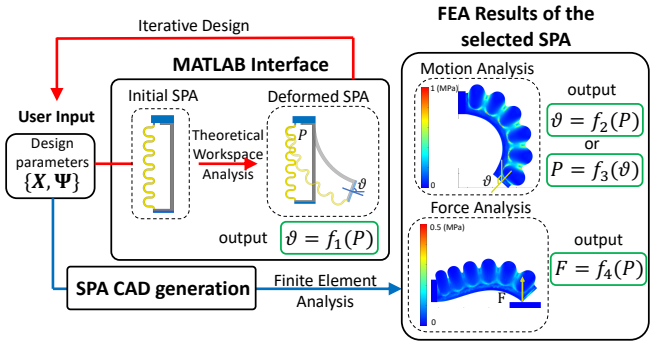

Fig. 1: The framework of the proposed bellow soft pneumatic actuator toolbox. The MATLAB interface takes user input, where $\mathbf{X}$ and $\mathbf{\Psi}$ represent the geometric and soft material parameters. The user-defined design parameters then update the initial bellow soft pneumatic actuator design schematic. The theoretical modelling analyses the SPA workspace for iterative design and outputs a relationship f_1 of the pressure P and angular deflection θ. The finite element modelling method takes the input of design parameters and generates a SPA CAD model. It analyses deformation and force in detail, and output relationship f_2, f_3 of P and θ as well as f_4 of P and blocked force F, respectively.

I. INTRODUCTION

Soft Pneumatic Actuator (SPA), made of elastomeric materials and actuated by pressurised air, has received particular interest from the soft robotic community due to its low cost, high compliance, flexibility in design and ease of control. SPAs have been designed in many different methods, targeting a variety of applications, including grasping [1], manipulation [2], and locomotion [3]. In general, SPAs can be categorised into ribbed, cylindrical and pleated types based on channel structure morphology [4]. This study mainly focuses on the bending SPA with the segment of pleated type or bellow type because it can be easily implemented with rapid prototyping. The bellow SPA refers to an actuator consisting of multiple hollow channels connected by a centre channel. When the fluid in the actuator is pressurised, due to the constraint layer at the bottom, each hollow channel would expand and cause the soft actuator to bend.

With the development of soft material 3D printing, the bellow SPAs are increasingly applied in recent studies [5]. Part of the main reason is that the currently available soft materials for 3D printing still do not meet the elasticity and elongation-at-break of conventional silicone rubbers [6], [7]. Thus, to maintain a larger deformation with minimum material stretch, a common solution for a 3D printed pneumatic actuator is to convert the material deformation to structural deformation. Bellow SPA is one of the promising designs for such implementation. The advantage is its capability of generating higher bending curvature and exerting higher maximum forces than ribbed and cylindrical morphology [4] as the bellow structure can provide a linear displacement by unfolding and ignoring the radial expansion [8]. The challenge is its requirements of the complex manufacturing process and higher shore hardness elastomer. However, this can be easily mitigated by 3D printing solutions.

Physical modelling is essential for the design of bellow SPAs. Udupa et al. [9] explored different bellow shapes and geometric parameters using beam theory and finite element analysis (FEA) simulation. Wang et al. [10] designed a soft gripper consisting of bellow SPA and analysed its performance using FEA. Without the physical modelling, the SPA needs to be tested with more in-depth experimental characterisations and developed with many trials of conceptual design iterations. Theoretical modelling is limited by the SPA geometry complexity, and differences in design features will lead to greater changes in the model. While FEA simulation has been widely used in soft robot analysis, it is still a difficult tool to use considering the wide range of parameter settings. All current works develop the simulation model for the actuator design with fixed design features/properties, making it difficult to be generalised. If others want to

*This work was supported by the Engineering and Physical Sciences Research Council (EPSRC) Grant EP/V000748/1;
[1] Yao Yao, Liang He and Perla Maiolino are with Oxford Robotics Institute, University of Oxford, Oxford, OX1 2JD, United Kingdom; *Corresponding Author: Liang He yao/liang/perla@oxfordrobotics.institute

2022 IEEE 5th International Conference on Soft Robotics (RoboSoft) | 978-1-6654-0828-8/22/$31.00 ©2022 IEEE | DOI: 10.1109/ROBOSOFT54090.2022.9762153

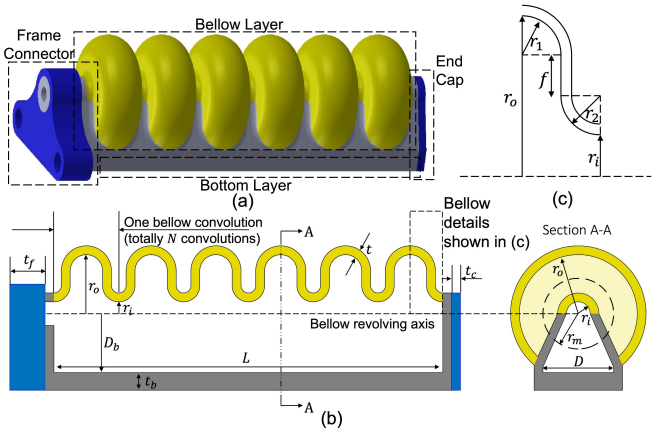

Fig. 2: The bellow SPA design. The 3D dimetric view is shown in (a). The front and sectional schematic view of the parameterised design is shown in (b), in which the colours represent the same parts as in (a), and the shallow yellow in the sectional view A-A is to show the radius of the revolved bellow changing from r_i to r_o. The enlarged half bellow convolution with detailed geometric parameters is shown in (c).

extend the design to achieve different workspace or force performance, they may need to go through a new process of design, simulation, prototyping, and validation.

Therefore, there is a need for a comprehensive design and analysis solution based on a standardised bellows design that allows the material properties and geometric parameters of the bellows SPA to be customised. A generalised design toolbox is an effective solution to significantly reduce the time the user spends on physical modelling and validation during actuator design. Design tools have already demonstrated their effectiveness for SPAs. Moseley et al. developed an FEA-based tool to facilitate the design of SPAs with ribbed channel structure and cast silicone as the material [11]. However, it is inapplicable for pleated actuators manufactured by soft 3D printing technologies.

This work is going to present a design toolbox for bending bellow SPAs with tunable geometric and material parameters that can analyse the actuator workspace via theoretical modelling for iterative design and further simulate the deformation and force performance by using FEA. In Section II, the design of the standardised actuator is introduced with key parameters. In Section III, the toolbox architecture and graphical user interface (GUI) are presented. In Section IV, the theoretical modelling and FEA modelling are detailed explained. In Section V, experimental results are shown to validate the modelling methods.

II. Actuators Design and Fabrication

A. Design Parameters

According to Wilson [12], there are mainly ten basic bellow configurations. Among those, the U-shaped bellow is selected in our design as it can compute maximum deflection for under the same input pressure [13].

The standardised bellow SPA design used in the proposed toolbox is shown in Fig.2(a). The bellow SPA is a combination of a revolved bellow layer (in yellow colour) and a flat bottom layer made of soft materials (in grey colour), attached by a frame connector and an end cap made of rigid materials

TABLE I: Design Parameters

Parameter	Symbol	Default Value
Effective Length	L	66 mm
Bellow Number	N	6
Average Radius	r_m	6mm
Inner Radius	r_i	2mm
Outer Radius	r_o	10mm
Upper Arc Radius	r_1	2.75mm
Lower Arc Radius	r_2	2.75mm
Flank Length	f	2.5mm
Distance to the Bottom	$D_b = ro$	10mm
Bottom Width	$D = 2r_m$	12mm
Bellow Wall Thickness	t	1.5mm
Bottom Thickness	$t_b = 2t$	3mm
Frame Connector Thickness	t_f	6mm
End Cap Thickness	$t_c = t$	1.5mm

(in blue colour) for characterisation. The design is parameterised according to its geometrical parameters as shown in Fig. 2(b)(c) and Table. I. The bellow layer consists of N of identical axis-symmetric bellow convolution. As shown in Fig. 2(c), half of each convolution can be parameterised by a 1/4 upper arc with radius r_1, a flank with length f, and a 1/4 lower arc with radius r_2. The effective length $L = 2N(r_1 + r_2)$ is defined as the total length of the bellow convolution. Fig. 2(b) indicates that the distance from the revolving axis to the lowest point of the bellow convolution is the inner radius r_i of the bellow, whereas the distance to the highest point is the outer radius r_o, and r_m is defined as the average radius ($r_m = \frac{1}{2}(r_i + r_o)$). The distance from the bellow revolving axis to the bottom layer is defined as $D_b = r_o$ and the width of the bottom layer is defined as $D = 2r_m$. In addition, the bellow wall thickness is defined as t, and the bottom layer thickness is $t_b = 2t$. The frame connector thickness is defined as t_f and the end cap thickness is $t_c = t$.

B. Fabrication of the SPAs

To validate the performance of the toolbox, the SPAs were printed using a commercially available 3D printer (PolyJet J735, Stratasys Inc., Minnesota, United States). This printer can conduct multi-material printing by mixing rigid materials such as the Vero family and soft materials such as Agilus30 to produce digital materials in a variety of flexible Shore A hardness. After printing, the support material SUP706 was removed by chemical bathing.

III. The Toolbox Architecture and Interface

The design toolbox is built using an interface between COMSOL MultiPhysics and MATLAB. Fig. 3 shows the GUI of the toolbox, where users can define critical design features and material properties. Theoretical analysis is used to simulate the 2D deformation of the SPA within a couple of seconds. Users can evaluate the actuator angular deflection in the interactive interface by manually control a slider to adjust the driving pressure. Once the user is satisfied with the SPA 2D workspace, detailed 3D FEA can be carried by click on the "Analyse" button. Subsequently, the design parameters and material properties will be sent to COMSOL with a CAD model generated. Simulation in structural mechanics

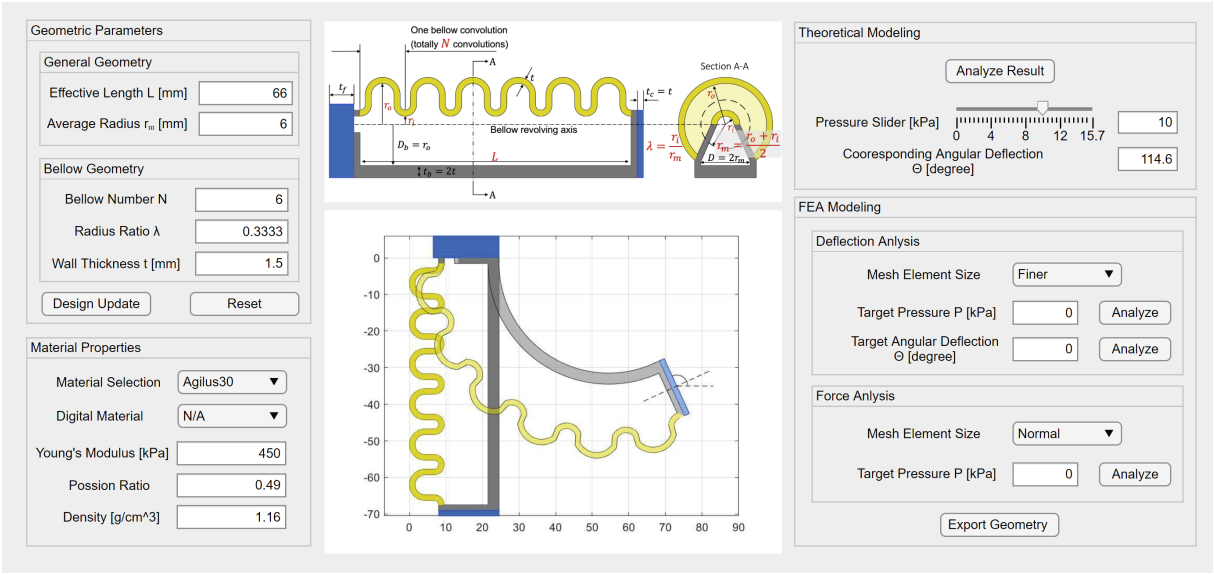

Fig. 3: The interface of the bellow SPA toolbox. The left upper section is the "Geometric Parameters" panel. The left bottom section is the "Material Proprieties" panel. The middle upper section shows the parameterised design of the bellow SPA to provide design guidance. The middle lower section is the design schematic diagram, showing the initial design of the bellow SPA and the deformed bellow SPA after theoretical modeling simulation. The right upper section is the "Theoretical Modeling" panel. The right lower section is the "Finite Element Analysis Modeling" section.

will be built in the background with the physics, boundary conditions, and mesh created. The GUI will then shows the detailed results of displacements, forces, stress and strains acquired via the FEA results (detail will be shown in Sec IV-B and Fig. 6). After inspecting the detailed FEA result of the SPA deformation and force output, the user can decide to generate an STL file for 3D printing of the actuator.

A. Geometric Parameters

The toolbox allows for setting critical geometrical parameters based on the design of the standardised bellow SPA, which is categorised in two aspects.

- The general SPA geometry: (a) effective length L. Default: 66mm. (b) average radius of the bellow r_m. Default: 6mm. These two parameters restrain the initial volume of the SPA.
- The bellow geometry: (a) number of the bellow convolution N. Default: 6. (b) the ratio of inner radius over average radius of the bellow $\lambda = r_i/r_m$. Default: 1/3. (c) wall thickness t. Default: 1.5mm. These three parameters would effect bellow's ability of unfolding.

The "Design Update" button checks the geometric constraints of the input and update the design schematic diagram; the "Reset" button would set all geometric parameters to the default value.

Aside from all the geometric parameters should be positive, the geometric constraints are the following: 1) the bellow number N must be a positive integer; 2) the wall thickness t can not exceed the upper or lower arc radius of the bellow, which equals to $L/4N$; 3) the difference between the outer radius r_o and inner radius r_i shouldn't be smaller than the sum of the upper and lower arc radius of the bellow.

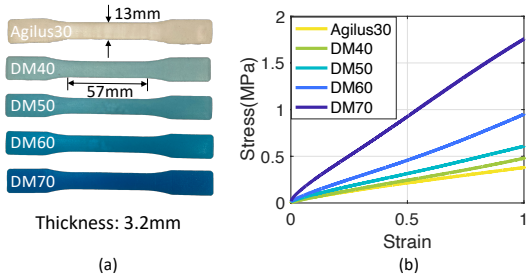

Fig. 4: Material characterization of Agilus30 and its digital materials. (a) Specimens for tensile tests. (b) Stress-Strain curves of the materials.

The equation form is

$$\begin{cases} N \in \mathbb{Z}^+ \\ t < \frac{L}{4N} \\ (1-\lambda) r_m \geq \frac{L}{4N} \end{cases} \tag{1}$$

B. Material Properties

In this paper, the toolbox provides two types of soft materials – Agilus30 and TangoPlus, and their digital materials mixed with the Vero family [14]. Three key material parameters are shown:

- The Young's Modulus $E = \sigma/\epsilon$, where σ and ϵ are the material's mechanical stress and strain. The standardised bellow SPAs undergo relatively small strain as the deformation is mainly due to the geometry unfolding. Thus, the SPA is modelled with a constant E to describe its elasticity where a linear elastic model is assumed for the theoretical model, and a neoHookean model is considered in the FEA. The selection of neoHookean model is based on its few parameters requirements and good agreement for small strain problem [15]. For TangoPlus and its digital materials, the material properties are extracted from the data found in literature [16]. For Agilus30 and its digital materials,

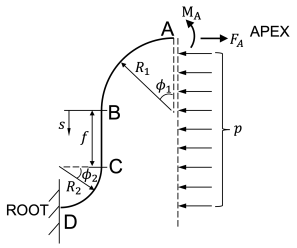

Fig. 5: Unit-width half bellow convolution modelled as guided cantilever beam

material characterisations were conducted with tensile tests of printed specimens. The specimens are shown in Fig.4(a), and the stress-strain curves are shown in Fig.4(b).

- The Poisson's ratio is a measure of the Poisson effect, the deformation of a material in directions perpendicular to the specific direction of loading. Default: 0.49.
- The density of the material, acquired via data sheet [14].

Material parameters will be updated automatically via drop-down selections in the GUI. Users can also characterise other materials or acquire data from literature/datasheets and input them into the GUI for simulation.

C. Simulation Methods

The toolbox simulation contains theoretical and FEA modelling. The theoretical modelling is based on the Beam Theory and Castigliano's Theorem [17]. Compared with FEA modelling, it can generate the SPA workspace in a short time (less than a minute). FEA modelling is based on COMSOL MultiPhysics, providing pressure-controlled and displacement-controlled simulation. The pressure-controlled simulation computes the angular deflection and blocked force depending on the input pressure, whereas the displacement-controlled simulation calculates the required pressure of the input target angular deflection. In addition, mechanical results such as detailed stress and strain of SPAs are also provided by the FEA modelling. The computation time of the FEA modelling varies depending on the complexity of the model. It takes 1 hour and 14 mins to finish simulating the deformation of SPA with default parameters under 10 kPa pressure. An Intel(R) Core(TM) i7-10875H CPU @ 2.30GHz computer processor with 16.0 GB RAM is used for simulation.

IV. Modelling and Simulation

A. Theoretical Modelling

The theoretical model is built based on the following assumptions: 1) the SPA deforms with approximately constant curvature [18], 2) the bottom layer is considered to be flexible and inextensible [5], 3) the SPA bends mainly due to the bellow unfolding to create a length difference between the bellow and bottom layer instead of radial expansion [8]. Based on these assumptions, the bending bellow SPA can be considered as a linear bellow actuator restrained one side. The ability of the bellow unfolding is related to the actuation pressure, the geometry of the bellow, and material properties. The linear bellow displacement under internal pressure can be modeled by treating each half bellow convolution as a unit-width guided cantilever beam as shown in Fig.5 [17].

The following assumptions are made for analysing the beam: 1) only consider the elastic situation, 2) deformation is only caused by bending strain energy, 3) the shift of the neutral axis of the beam is neglected during deformation, $R_1 = r_1 + \frac{t}{2}$ and $R_2 = r_2 - \frac{t}{2}$, 4) there is no rotation at A and D, 5) the vertical component of the pressure load is eliminated in the analysis, since the radial expansion of the bellow is neglected [19]. Therefore, the bending moment for each region of the beam is:

$$M_1 = M_A + p\frac{R_1^2(1-\cos\phi_1)^2}{2} - F_A R_1(1-\cos\phi_1) \quad (2)$$

$$M_2 = M_A + p\frac{(s+R_1)^2}{2} - F_A(s+R_1) \quad (3)$$

$$M_3 = M_A + p\frac{(R_1+f+R_2\sin\phi_2)^2}{2} - F_A(R_1+f+R_2\sin\phi_2) \quad (4)$$

where the subscript 1,2,3 stand for arc AB, flank BC and arc CD, respectively. The bending strain energy is

$$U = \frac{\int_0^{\frac{\pi}{2}} M_1^2 R_1 \mathrm{d}\phi_1 + \int_0^f M_2^2 \mathrm{d}s + \int_0^{\frac{\pi}{2}} M_3^2 R_2 \mathrm{d}\phi_2}{2EI} \quad (5)$$

where $I = \frac{1}{12}t^3$ is the unit-width second moment of inertia. According to Castigliano's theorem, the rotation φ and axial displacement δ_x at A are defined as

$$\varphi = \frac{\partial U}{\partial M_A} = 0 \quad (6)$$

$$\delta_x = \frac{\partial U}{\partial F_A} \quad (7)$$

From the symmetry of the bellow convolution and the pressure load on the end cap of the linear bellow

$$F_A = \frac{p(R_1+f+R_2)}{2} + \frac{p\pi r_i^2}{2\pi r_i} \quad (8)$$

The length difference between the bellow layer and constrained layer is $\Delta L = N\delta_x/b$, where b is a free parameter that allows adjustment of the length difference so that it can better match with experimental results. Then the angular deflection Θ of the bending bellow SPA is the length difference ΔL divided by the distance from the bellow highest point to the bottom of the actuator.

$$\Theta = \frac{\Delta L}{2r_o + t_b} \quad (9)$$

B. FEA Modelling on COMSOL

The FEA Modelling with COMSOL MultiPhysics contains SPA's deformation and force performance evaluation.

The simulation of deformation is built in the following steps: 1) Create a 3D solid mechanics physics model of stationary study type. 2) Define geometric and material parameters in Global Definitions. 3) Build the 3D geometry model. 4) Define materials and assign them to the corresponding domains. Use mixed "Pressure formulation" in

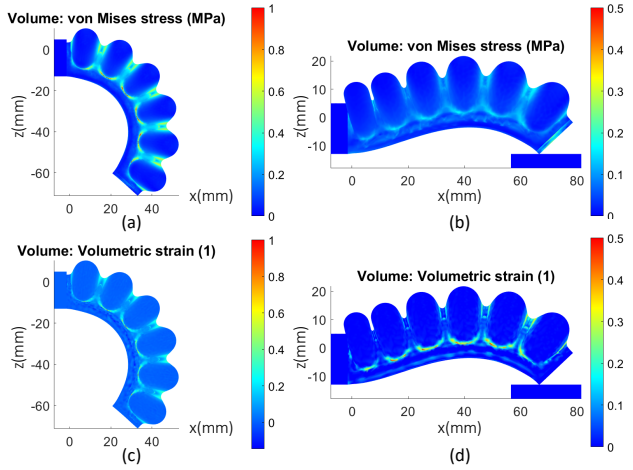

Fig. 6: The FEA results of the example bellow SPA at 10 KPa, including the stress distribution of the deformation simulation (a) and the force simulation (b), together with the strain distribution of the deformation simulation (c) and force simulation (d).

Solid Mechanics → Linear Elastic Material. Apply "Neo-Hookean" model on the soft domain. 5) Add boundary conditions. The pressure load "P" is defined in Global Definitions. 6) Mesh SPA with default element size "Finer" and build. In the toolbox, users can also change mesh size to get a more accurate result or less computational time. 7) Create stationary Study 1 for pressure control simulation: use range(0, P_s, P_f) to ramp "P", where "P_f" and "P_s" are defined as the target pressure and simulation interval; Use "Suggested Direct Solver (solid)" as the linear solver and select "MUMPS" solver; Set "Constant Newton" and "Anderson acceleration" as the nonlinear method. 8) Create stationary Study 2 for displacement control simulation: use range(0, d_s, d_f) to ramp the edge displacement "d", where "d_f" and "d_s" are defined as the target displacement and simulation interval. Before that, create an Average operator in Component → Definitions and select the end bottom edge as an entity. Next, in the Solid Mechanics → Global Equation, define "aveop(-u)-d" as the equation and "P" as the dependent variable.

The simulation of blocked force is modelled similarly except: 3) Add a cylinder adhered to the end of the bottom layer. Form the whole geometry as an assembly with a contact pair. 5) Define contact pairs in Component → Definitions. Add contact pair condition under Solid Mechanics. 6) Select mesh size "Normal". 7) In this case, we only use the pressure control simulation.

Fig.6 shows the FEA results of the example bellow SPA using the default geometry and material settings (see Sec. III-A and III-B) acquired via the toolbox. Both the deformation and stress/strain can be observed. Compared with the tensile strength of 2.4 - 3.1 MPa and elongation-at-break of 220 - 270% of Agilus30 [20], the resultant maximum von mises stress and maximum volumetric strain shown in Fig. 6 indicates that the example bellow SPA should be safe under the pressure of 10 kPa.

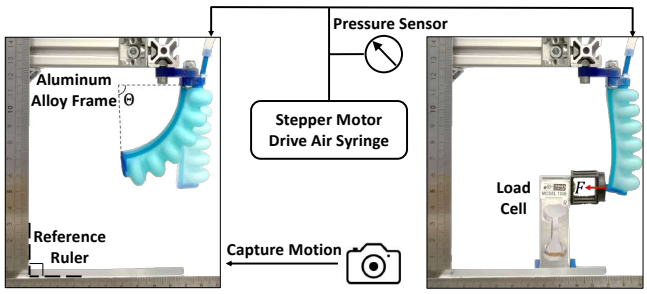

Fig. 7: The experimental set up to verify the simulation results of deformation (left) and force (right) analysis.

V. Experiments Validation and Discussion

To validate the analysis results provided by the toolbox, we designed and conducted experimental characterisation. In the experiment, the driving pressure of the SPA is selected as from 0 to 10kPa. Different design parameters are tested to verify the model accuracy, while experiments of both deformation and force are designed in three groups: changing the bellow number N, radius ratio $\lambda = r_i/r_m$ and the material stiffness, with respect to the default design parameters. The effective length and average radius of all prototypes are kept as the same: $L = 66$mm, $r_m = 6$mm. For each prototype, the experiment was conducted 5 times repeatedly.

Fig. 7 shows the experiment setup, where the bellow SPA was fixed by connecting the frame connector to an Aluminum alloy frame. A pneumatic system consisting of a 12V DC stepper motor driving a 60mL air syringe, a microcontroller (Arduino Mega), a pressure sensor (ADP51A11, pressure range 0-40 kPa, Panasonic, Japan), and a PI controller is used to control the driving pressure of the SPA. In each test, the pressure sensor is used as feedback to conduct close loop control of the output pressure and data is collected after pressure stabilising for 30 sec to minimise material hysteresis. In the experiments of SPA deformation, the angular deflection Θ is defined as the angle between the frame connector and the end cap. A RealSense camera (Intel, USA) is used to capture the deflection angle, which is calculated by MATLAB image processing toolbox using the frame connector end cap's pixel coordinates. A right-angle reference ruler was attached to the Aluminum alloy frame to provide calibration of the camera image. In the blocked force experiments, a load cell (Model 1006, Tedea-Huntleigh) with amplifier (HX711, SparkFun, United States) is used to collect the force data via the microcontroller. We took average measurement of 200 readings after pressure stabilised for 30 seconds, which lasted about 20 seconds.

To match the data provided by the theoretical modelling with the experimental results, we find the free parameter b defined in Sec. IV-A works well when $b \sim \frac{\lambda^{0.3}}{N^{0.9}.E^{0.6}}$. Fig.8 shows the comparison between the toolbox simulation and the experimental result. In the results of deformation, both modelling methods fit the tendency of experimental data. Due to gravity, the experimental and FEA results have an offset at 0 kPa, and the theoretical model does not take this into account, so it starts from 0°. Compared to the experimental result, the root mean square error (RMSE) for the FEA

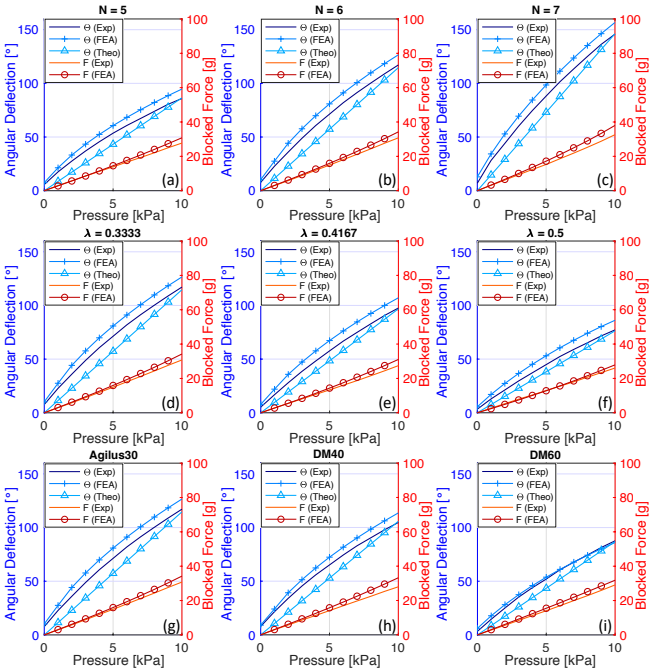

Fig. 8: The comparison of results from experiment and modelling of both deformation and force: the group of changing bellow number N, radius ratio λ and soft material are shown in (a-c), (d-f) and (g-i), respectively.

simulation and theoretical modelling are 9.00° and 7.40°, respectively.

As for the blocked force comparison, the FEA results also show a similar trend to the experimental ones. In all cases, the deviation of the FEA results from the experimental data increases as the pressure increases, which leads to an increasing error. The RMSE of the FEA simulation is 1.66 g. In general, the modelling results of deformation and force are in good agreement with the experimental results, which indicates the toolbox is reliable.

Furthermore, the toolbox has some limitations. First of all, it analyses the SPA performance based on the quasi-static equilibrium assumption. Secondly, it only considers newly manufactured prototypes, although SPA performance will vary with age. Besides, it doesn't provide information about the durability of the design actuators. However, the paper of Dämmer et al. [21], provides insights about the relationship between load cycles to failure and finite element simulated maximum principal strain on the PolyJet bellows actuators. Suppose users are interested in the durability of the bellow actuator. In that case, they can look at the strain results from the finite element simulation in the toolbox and compare them with the work in [21].

VI. Conclusion

This paper describes a toolbox for the design and analysis of the bellow soft pneumatic actuator and discusses its limitations. The toolbox aims to expedite the digital design process of bellow SPAs with a package containing the customisation of geometric/material parameters, fast theoretical modelling (based on Beam Theory and Castigliano's Theorem), detailed FEA modelling (based on COMSOL Multiphysics), and the SPA CAD for direct 3D printing. Experimental results of the angular deflection and blocked force of the selected SPAs in three dimensions of design parameters is conducted, validating the toolbox with maximum RMSE of 9.00°, 7.40° and 1.66 g for the theoretical modelling of deformation, FEA modelling of deformation and force, respectively. Future work of the design toolbox would focus on introducing multi-objective design optimisation to user-defined tasks.

References

[1] R. Deimel and O. Brock, "A novel type of compliant and underactuated robotic hand for dexterous grasping," *The International Journal of Robotics Research*, vol. 35, no. 1-3, pp. 161–185, 2016.

[2] L. He, X. Tan, K. Suzumori, and T. Nanayakkara, "A method to 3d print a programmable continuum actuator with single material using internal constraint," *Sensors and Actuators A: Physical*, vol. 324, p. 112674, 2021.

[3] A. D. Marchese, C. D. Onal, and D. Rus, "Autonomous soft robotic fish capable of escape maneuvers using fluidic elastomer actuators," *Soft Robotics*, vol. 1, no. 1, pp. 75–87, 2014. PMID: 27625912.

[4] A. D. Marchese, R. K. Katzschmann, and D. Rus, "A recipe for soft fluidic elastomer robots," *Soft Robotics*, vol. 2, no. 1, pp. 7–25, 2015. PMID: 27625913.

[5] A. Zolfagharian, M. A. P. Mahmud, S. Gharaie, M. Bodaghi, A. Z. Kouzani, and A. Kaynak, "3d/4d-printed bending-type soft pneumatic actuators: fabrication, modelling, and control," *Virtual and Physical Prototyping*, vol. 15, no. 4, pp. 373–402, 2020.

[6] J. Herzberger, J. M. Sirrine, C. B. Williams, and T. E. Long, "Polymer design for 3d printing elastomers: Recent advances in structure, properties, and printing," *Progress in Polymer Science*, vol. 97, p. 101144, 2019.

[7] O. Shorthose, L. He, A. Albini, and P. Maiolino, "Design of a multi-material 3d-printed soft actuator with bi-directional variable stiffness," in *Annual Conference Towards Autonomous Robotic Systems*, pp. 238–248, Springer, 2021.

[8] R. Hashem, M. Stommel, L. Cheng, and W. Xu, "Design and characterization of a bellows-driven soft pneumatic actuator," *IEEE/ASME Transactions on Mechatronics*, pp. 1–1, 2020.

[9] G. Udupa, P. Sreedharan, P. Sai Dinesh, and D. Kim, "Asymmetric bellow flexible pneumatic actuator for miniature robotic soft gripper," *Journal of Robotics*, vol. 2014, no. 902625, 2014.

[10] Z. Wang and S. Hirai, "Chamber dimension optimization of a bellow-type soft actuator for food material handling," in *2018 IEEE International Conference on Soft Robotics (RoboSoft)*, pp. 382–387, 2018.

[11] P. Moseley, J. M. Florez, H. A. Sonar, G. Agarwal, W. Curtin, and J. Paik, "Modeling, design, and development of soft pneumatic actuators with finite element method," *Advanced Engineering Materials*, vol. 18, no. 6, pp. 978–988, 2016.

[12] J. Wilson, "Mechanics of bellows: A critical survey," *International Journal of Mechanical Sciences*, vol. 26, no. 11, pp. 593–605, 1984.

[13] H. F. Lau, "3D-Printed Inflatable Actuators:Design and Development of Soft Actuators for a Pneumatically-Actuated Soft Robotic Arm," Master's thesis, ETH Zurich, Zurich, Switzerland, 2019.

[14] Stratasys, *Digital Materials Data Sheet*, 2020.

[15] M. S. Xavier, A. J. Fleming, and Y. K. Yong, "Finite element modeling of soft fluidic actuators: Overview and recent developments," *Advanced Intelligent Systems*, vol. 3, no. 2, p. 2000187, 2021.

[16] V. Slesarenko and S. Rudykh, "Towards mechanical characterization of soft digital materials for multimaterial 3d-printing," *International Journal of Engineering Science*, vol. 123, pp. 62–72, 2018.

[17] R. Chipman, R. Galantine, J. Susnir, U. A. E. Commission, and N. A. A. A. I. Division, *Stress Analysis of Bellows for the HNPF Intermediate Heat Exchanger*. AEC research and development report, Atomics International, 1962.

[18] G. Zhong, Y. Hou, and W. Dou, "A soft pneumatic dexterous gripper with convertible grasping modes," *International Journal of Mechanical Sciences*, vol. 153-154, pp. 445–456, 2019.

[19] N. Murray, "Stress analyses of wrinkle bends in pipelines," *Thin-Walled Structures*, vol. 17, no. 1, pp. 65–80, 1993.

[20] Stratasys, *Agilus30 Materials Data Sheet*, 2020.

[21] G. Dammer, S. Gablenz, A. Hildebrandt, and Z. Major, "Polyjet-printed bellows actuators: Design, structural optimization, and experimental investigation," *Frontiers in Robotics and AI*, vol. 6, p. 34, 2019.